Article

Highly reliable low threshold InAs quantum dot lasers on on-axis (001) Si with 87% injection efficiency

Daehwan Jung, Zeyu Zhang, Justin Norman, Robert Herrick, MJ Kennedy, Pari Patel, Katherine Turnlund, Catherine Jan, Yating Wan, Arthur Gossard, and John E. Bowers

ACS Photonics, **Just Accepted Manuscript** • DOI: 10.1021/acsphotonics.7b01387 • Publication Date (Web): 18 Dec 2017

Highly reliable low threshold InAs quantum dot lasers on on-axis (001) Si with 87% injection efficiency

Daehwan Jung[1,*], Zeyu Zhang[2,*], Justin Norman[3], Robert Herrick[4], MJ Kennedy[2], Pari Patel[2], Katherine Turnlund[1], Catherine Jan[4], Yating Wan[2], Arthur C. Gossard[1,2,3], John E. Bowers[1,2,3]

*Equal contribution

[1]Institute for Energy Efficiency, University of California Santa Barbara, Santa Barbara, CA, USA, 93106
[2]Department of Electrical and Computer Engineering, University of California Santa Barbara, Santa Barbara, CA, USA, 93106
[3]Materials department, University of California Santa Barbara, Santa Barbara, CA, USA, 93106
[4]Intel Corporation, Santa Clara, CA, USA, 95054

Abstract: Quantum dot lasers epitaxially grown on Si are promising for an efficient light source for silicon photonics. Recently, considerable progress has been made to migrate 1.3 μm quantum dot lasers from off-cut Si to on-axis (001) Si substrate. Here, we report significantly improved performance and reliability of quantum dot lasers enabled by a low threading dislocation density GaAs buffer layer. Continuous-wave threshold currents as low as 6.2 mA and output powers of 185 mw have been achieved at 20 °C. 1500-hour reliability tests at 35 °C showed an extrapolated mean-time-to-failure of more than a million hours. Direct device transparency and amplified spontaneous emission measurements reveal an internal optical loss as low as 2.42 cm^{-1} and injection efficiency of 87%. This represents a significant stride toward efficient, scalable, and reliable III-V lasers on on-axis Si substrates for photonic integrate circuits that are fully compatible with CMOS foundries.

1. Introduction

Semiconductor lasers utilizing self-assembled InAs quantum dots (QDs) as an active medium have shown promise as an efficient light source for silicon photonics and have achieved significant advances over the past decades.[1] Due to effective lateral carrier confinement in the self-assembled nanostructures, QD lasers grown on Si have proven their superior performance over the conventional quantum well lasers on Si in terms of lower threshold current, higher efficiency, and more reliable operation.[2-4] Most of the previous QD lasers epitaxially grown on Si employed 4-6 ° off-cut Si substrates to suppress anti-phase domains that can readily form in the interface between III/V and Si and that can drastically degrade device performance.[5] Recently, use of on-axis (001) Si substrates has drawn much attention since they are compatible with current CMOS foundries.[6-8] However, past QD lasers grown on on-axis Si not only have shown diminished performance in terms of high threshold current and low output power, but also have left the device reliability as an unresolved issue.

We have recently demonstrated low threshold and high efficiency QD lasers epitaxially grown on on-axis Si.[9] We believe that the dramatically reduced threading dislocation density from ~3×10^8 cm^{-2} to ~7×10^6 cm^{-2}, enabled the high performance compared to previous reports. However, no in-depth laser characterization on the epitaxially grown QD lasers on Si has been conducted, although understanding the laser physical parameters such as injection efficiency, optical loss, and transparency current should lead to further advancement in the QD lasers on Si. Also, there has been no report about the reliability of the QD lasers grown on on-axis (001) Si with the low threading dislocation density.

Here, we report optical characteristics of high performance QD lasers epitaxially grown on on-axis (001) Si substrates using molecular beam epitaxy (MBE). InGaAs/GaAs strained layer superlattices and thermal cyclic annealing were employed to effectively reduce the threading dislocation density in the GaAs buffer

layer to 8.4 × 10^6 cm^{-2}. QD lasers grown on the high-quality GaAs/Si template demonstrate ultra-low continuous-wave (CW) threshold current of 6.2 mA, high power of 185 mW, and wall-plug efficiency as high as 31% at 20 °C. Optical characterizations on the QD devices grown on Si were performed to understand the performance improvement, and we have achieved transparency current density of 13 A/cm^2 per QD layer, internal optical loss of 2.42 cm^{-1}, and injection efficiency of 87%. Finally, the high performance QD lasers on Si also show superior reliability with extrapolated mean-time-to-failure of more than a million hours for CW operation at 35 °C, demonstrating the first reliable operation of lasers epitaxially grown on CMOS compatible on-axis (001) Si.

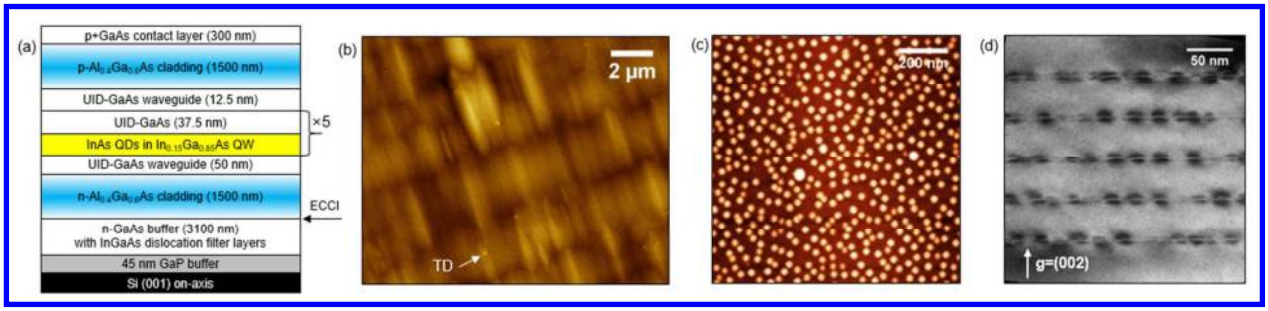

Figure 1 (a) Schematic of GaAs/AlGaAs separate confinement heterostructure laser diode grown on GaAs buffer layer on Si. (b) Electron channeling contrast image to show threading dislocations on the GaAs buffer layer. One of the threading dislocations is indicated by an arrow. (c) Atomic force microscopy image of quantum dots with a density of 4.9 × 10^{10} cm^{-2}. (d) Cross-sectional bright-field transmission electron microscopy image of coherently grown five layers of quantum dot active region in the laser epi material. The two-beam condition used in the image is **g**= (002).

The samples were grown by solid-source MBE. Figure 1 (a) illustrates the entire QD separate confinement heterostructure grown on a Si substrate, which was purchased from $NAsP_{III/V}$ GmbH. The Si substrate has a 45-nm thick pseudomorphic GaP buffer layer. Antiphase domains that form at the GaP and Si interface terminate within the 45 nm GaP layer due to the special Si surface preparation before the GaP epitaxy.[10] A 100 nm thick low-temperature GaAs layer was first grown at 500 °C at a growth rate of 0.1 μm/hr after oxide desorption. The substrate temperature was raised to 600 °C to grow a 1.5 μm GaAs layer at 1 μm/hr growth rate. Then, the growth was interrupted and thermal cycle annealing was performed four times between 320 °C and 700 °C under As_2 overpressure. A superlattice of 10 pairs of 20 nm $In_{0.1}Ga_{0.9}As$/10 nm GaAs was grown at 500 °C as a dislocation filter after the annealing, and a 700 nm n-type GaAs cap layer was grown to complete the buffer growth. The sample was removed from the chamber to analyze the threading dislocation density and surface roughness. Figure 1 (b) shows an electron channeling contrast image (ECCI) of the GaAs buffer layer on the Si substrate. The channeling condition used in the imaging is a cross-point of (220) and (400) patterns to avoid dislocation invisibility criteria. Threading dislocations are clearly seen as bright or dark spots in the image. The threading dislocation density was found to be 8.4 × 10^6 cm^{-2} by surveying a ~4500 μm^2 scan area. The smooth surface morphology of the GaAs buffer layer was confirmed by atomic force microscopy measurement with root-mean-square roughness of 2.6 nm.

Figure 1 (c) shows highly uniform InAs QDs grown on the GaAs/Si template. More information about the QD growth condition can be found elsewhere.[9] The density of the uncapped QDs is ~4.9 × 10^{10} cm^{-2}. The average QD height is 11.5 nm with a standard deviation of 2.1 nm, confirming highly homogeneous

height distribution of the QDs grown on Si substrates (See S.I.). Bright-field transmission electron microscope (X-TEM) image of Figure 1 (d) shows five stacks of the QD layers in the laser structure. The X-TEM image reveals coherently grown QD layers. Also, the QDs are not vertically coupled to each other due to the relatively thick GaAs spacing layer (37.5 nm). The absence of threading dislocations in the X-TEM image further confirms that the density of threading dislocations in the QD active region is below the detection limit, which is typically 1×10^7 cm^{-2}.

The as-grown material was processed into ridge-waveguide lasers with various device widths using standard dry-etching techniques. The cavity length was determined by cleaving after thinning the backside of the Si substrate to ~150 μm. All light-current-voltage (LIV) measurements presented in this work were measured in the CW mode at 20 °C, and threshold currents from 55 devices are displayed in Figure 2 (a). The threshold current is linearly decreased with device width down to 2.5 μm. The inset reveals a threshold current of 8.7 mA from a 2.5×1341 μm^2 device. The lowest threshold current density is 198 A/cm^2 at 20 °C and the highest wall-plug efficiency is 31%. (See S.I.) Applying high-reflectivity (8 pairs of SiO_2 and Ta_2O_5) coatings on one facet further reduced the threshold current, and Figure 2 (b) shows a CW threshold current of 6.2 mA, demonstrating the lowest threshold current among any Fabry-Perot lasers epitaxially grown on Si to date. Thermal performance was also assessed and Figure 2 (c) shows that the CW ground-state lasing from a QD laser (8×1341 μm^2 device) persists up to 85 °C with an output power of ~8 mW, which is the highest ground-state CW lasing for QD lasers grown on on-axis Si. The calculated characteristic temperature is 29.8 K. This relatively low characteristic temperature can be improved by incorporating p-modulation doping in the active region.[11] The QD laser produced high output powers up to 185 mW at 20 °C. (See S.I.). We believe that the high performance QD lasers with the low threshold current and high output power were enabled by the significantly reduced threading dislocation density in the QD active region.

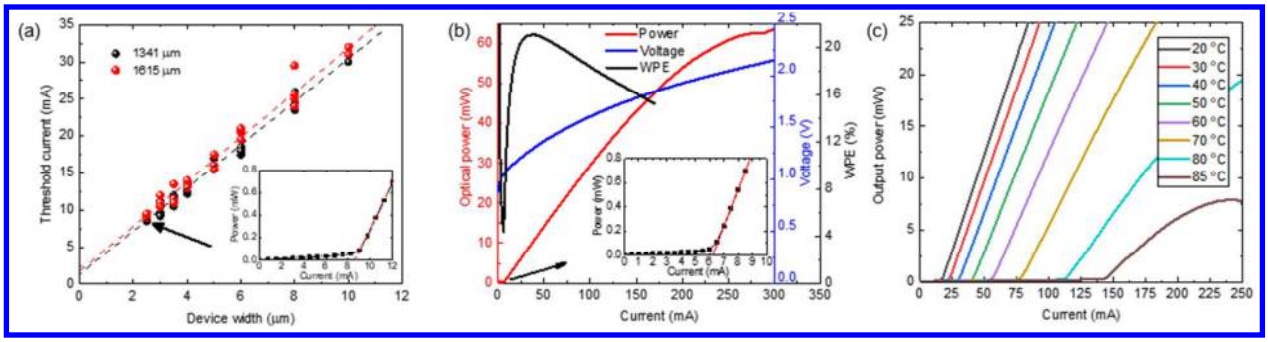

Figure 2 (a) Continuous-wave (CW) threshold current versus device width plot at 20 °C for two cavity lengths (As-cleaved facets). The dashed lines are linear fittings and the inset shows threshold current of 8.7 mA from a 2.5×1341 μm^2 device. (b) CW LIV and wall-plug-efficiency plots from a 2.5×1079 μm^2 device at 20 °C show a 6.2 mA threshold current and 21% single-side peak efficiency. (c) LIV curves versus heat sink temperatures.

To further understand the effect of material improvement on the laser performance, comprehensive gain characteristics, loss mechanism, and injection efficiency have been investigated on the QD lasers epitaxially grown on Si. Inside a Fabry-Perot laser cavity, the below-threshold amplified spontaneous emission (ASE) spectrum can be described by[12]:

$$A(\lambda) = \frac{B(1+r_1 r_2 e^{(\Gamma G-\alpha_{\text{int}})L})(1-r_1 r_2)}{(1+r_1 r_2 e^{(\Gamma G-\alpha_{\text{int}})L})^2 - 4 r_1 r_2 e^{(\Gamma G-\alpha_{\text{int}})L} \cdot \sin^2(\frac{2\pi n L}{\lambda})}, \quad (1)$$

where B is the proportion of the total amount of ASE coupled into the cavity mode; r_1 and r_2 are the reflectivity of the mirror; Γ is the confinement factor of the active region; G is the material gain of the active medium; α_{int} is the internal loss; L is the cavity length; n is the effective index of the waveguide; and λ is the wavelength of spontaneous emission. Based on Eq. (1), the net modal gain (g_{net}) can be calculated based on[13]:

$$g_{\text{net}} = \Gamma G - (\alpha_{\text{int}} + \alpha_{\text{m}}) = \frac{1}{L} \ln \frac{y(\lambda)-1}{y(\lambda)+1}, \quad (2)$$

where $\alpha_{\text{m}} = \frac{1}{L} \ln \frac{1}{r_1 r_2}$ is the mirror loss of the laser cavity, $y(\lambda)$ is the ratio of the integral across one free spectral range (FSR) of the ASE spectrum over the cavity mode minimum[12]:

$$y(\lambda) = \frac{\int_{\lambda_1}^{\lambda_2} A(\lambda')\mathrm{d}\lambda'}{A_{min}(\lambda) \cdot (\lambda_2 - \lambda_1)}. \quad (3)$$

This method is properly named as the mode-sum method[13]. To implement it, the ASE spectra from a group of lasers with selected variation of lengths and widths were measured at sub-threshold bias conditions by coupling light out of the laser cavity through a lensed single mode fiber to an optical spectrum analyzer (OSA) with a resolution of 20 pm. The exemplary ASE measurement results for a 3.5 × 1341 μm^2 laser at 10.5 mA are displayed in Figure 3 (a). The same measurement was repeated by varying the bias current from 3.5 mA to 14 mA. Next, the gain spectrum was calculated based on the Eq. (2) and (3). The results are shown in the Figure 3 (c) inset. The device lased around the wavelength of the gain spectrum peak (in this case 1298.6 nm) at threshold. At this wavelength, the gain versus current relationship was plotted and shown in Figure 3 (c). The extracted data points show gradual decrease in the differential gain as the bias increases, and closely match a logarithmic gain-current relationship.

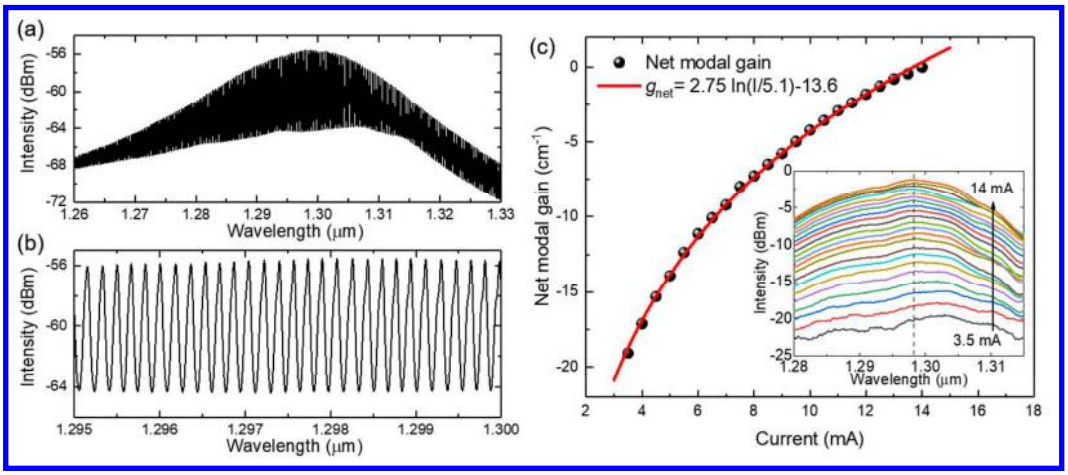

Figure 3. Net modal gain measurement and calculation. (a) ASE spectrum of a 3.5 × 1341 μm^2 laser. (b) a close-up view of the longitudinal modes in the ASE spectrum. (c) Calculated net modal gain at 1298.6 nm of the device. The inset shows the net modal gain spectrum of the device, where the dotted line marks the wavelength of the gain spectrum peak at the threshold.

Since the gain-current relationship has been determined to be logarithmic, the net modal gain can be modeled as:

$$g_{\text{net}} = g_0 \ln \frac{I}{I_{\text{tr}}} - g_{\text{th}} \quad (4)$$

where g_0 is the gain parameter, I_{tr} is the device transparency current, and $g_{\text{th}} = \alpha_{\text{int}} + \alpha_{\text{m}}$ is the threshold modal gain. It is clear from Eq. (4) that when the gain material reaches transparency, the absolute value of the net modal gain equals the threshold gain (i.e. total optical loss) of the laser. Therefore, by combining the transparency measurement with the mode-sum method, the gain and loss characteristics of the laser can be separated, and accurate optical loss can be reliably extracted. When a laser reaches transparency, the active material changes from an absorber to an amplifier, which implies a change of polarity in the photon induced current. Additionally, since the light-matter interaction is the weakest around transparency, the photon induced current should be minimum.[14] The measurement setup is shown in Figure 4 (a). When measuring the transparency, an externally modulated tunable laser source (TLS) was used to optically probe the device under test (DUT). The alternating current (AC) signal from the electrode of the laser was detected by a lock-in amplifier. It is worth mentioning that the transparency current was uniquely defined by the wavelength of the probing light[14, 15]. Therefore, the TLS was always tuned to the wavelength of the gain spectrum peak of DUT right before lasing. The measurement results for the same laser used for ASE measurement are shown in Figure 4 (b). Based on the foregoing analysis, the laser reaches transparency at 5.1 mA.

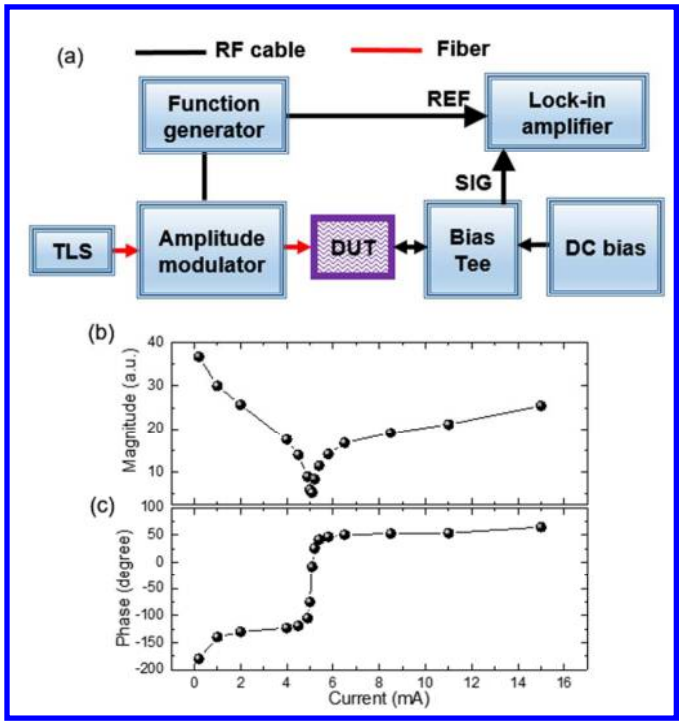

Figure 4. (a) Schematic representation of the transparency current measurement setup. (b) The magnitude and phase of the AC signal detected by the lock-in amplifier for the 3.5 × 1341 μm^2 laser when probed at 1298.6 nm.

Knowing the transparency current, the threshold gain of this laser is determined to be 13.6 cm^{-1} from Figure 3 (c). The gain parameter g_0 is extracted to be 13.8 cm^{-1} (2.75 cm^{-1} per QD layer) by Eq. (4). The

coefficient of determination (R^2) is 99.9 %, reaffirming the accuracy of the model. Assuming a commonly accepted value of 0.32 for the power reflectivity of the semiconductor-air interface after cleaving, the mirror loss for this laser (length 1341 μm) is 8.5 cm^{-1}. Thus, the internal loss is found to be 5.1 cm^{-1}. Finally, the injection efficiency (η_i) can be determined from the slope efficiency (SE), which is expressed as:

$$SE = \eta_i \frac{h\nu}{q} \frac{\alpha_m}{g_{th}} \quad (5)$$

where h is the Planck's constant, ν is the lasing frequency, q is the electron charge and η_i is the injection efficiency. For the same laser used in the gain and transparency measurement, η_i is calculated to be 74% for $SE = 0.442$. The parameter extraction procedure outlined above has a few advantages over the more commonly employed cutback method,[16-18] and more detailed discussion can be found in S.I.

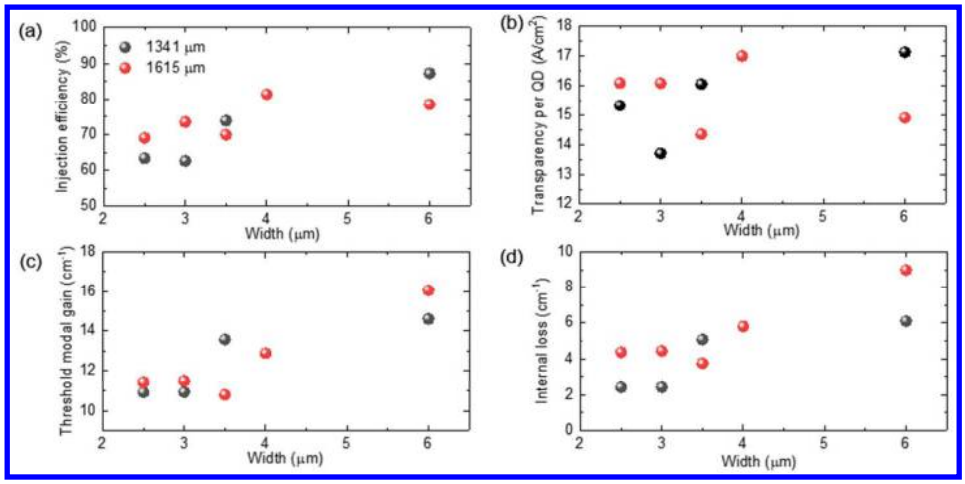

Figure 5. Extracted laser parameters as a function of ridge width. (a) Injection efficiency, (b) transparency current density per QD layer, (c) Threshold modal gain, and (d) Internal loss.

The parameter extraction results are summarized in Figure 5. The average material gain parameter g_0 is 2.46 cm^{-1} with a small standard deviation of 0.2 cm^{-1} across all the tested devices, confirming the consistency of our measurements. The highest injection efficiency of 87% was achieved from a 6 × 1341 μm^2 as shown in Figure 5 (a). Smaller ridge width devices show decreasing injection efficiencies probably due to the increased surface recombination. Transparency current density per QD layer was also deduced from the directly measured transparency current multiplied by the injection efficiency of each device, and the average is only 15.6 A/cm^2 with the lowest value of 13.1 A/cm^2, which is comparable to QD lasers on GaAs substrates (~10 A/cm^2).[19] The increase of threshold modal gain with ridge width (Figure 5(c)) is observed in conjunction with the blue shift of the lasing wavelength by ~7.5 nm as the ridge width is increased from 2.5 μm to 6 μm. The blue shift in the peaks of the gain spectra, also shown in the Figure 3 (c) inset, is caused by the increased quasi fermi level separation at high current injection, which allows the shallow dot population to contribute more to the gain spectrum. The rise of the threshold modal gain with ridge width is clearly similar to internal loss shown in Figure 5 (d). However, the reason behind the increased internal loss in wider lasers needs further investigation. It is worth mentioning that the injection efficiency of 87% achieved in some of our QD lasers epitaxially grown on Si is comparable to the ones grown on native GaAs substrates.[20] The maximum modal gain of 16.1 cm^{-1} was achieved from

the 6 × 1615 μm^2 device while the lowest internal loss of 2.4 cm^{-1} was observed from the 2.5 × 1341 μm^2 device.

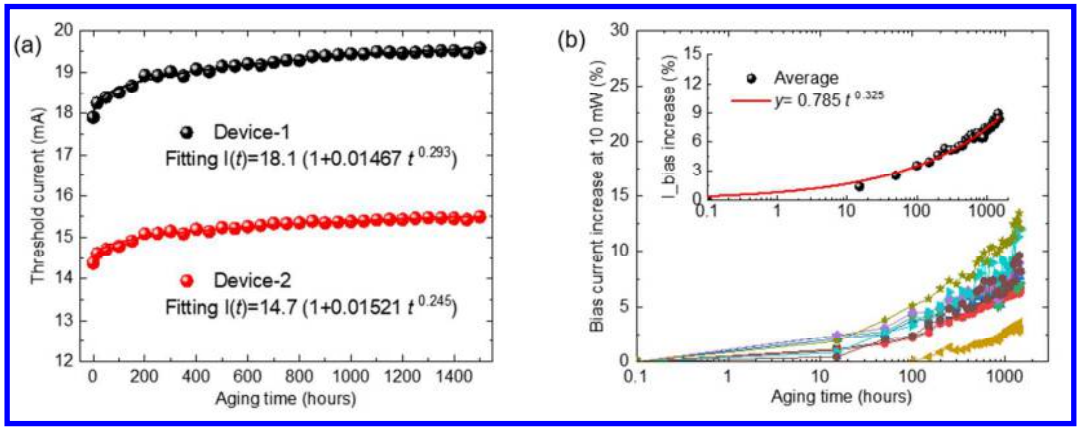

Figure 6 (a) Evolution of CW threshold current increases during 1500-hour lifetime test of two exemplary 1641 μm long devices. The solid lines are non-linear fittings with R-squared values of 0.983 and 0.979. (b) Bias current increases required to produce 10 mW output power under CW at 35 °C during the lifetime test. The inset is an average of 10 aged devices with a power fit.

QD lasers processed from the same batch of epi growth were prepared for lifetime measurements. The devices were mounted onto AlN carriers and wirebonded after applying high-reflectivity (8 pairs of SiO_2 and Ta_2O_5) coatings on one facet. Then, the carriers were shipped to Intel Corp. to age the devices at 35 °C under constant CW diving current. The aging current was varied from 30 mA to 70 mA depending on the carriers, which results in 1.6-2.4 times the initial threshold currents of each device. LIV sweeps were performed periodically to monitor the degradation rate during the aging. Figure 6 (a) displays gradual increases in the threshold currents from two of the QD lasers grown on Si over 1500-hour aging time. The threshold current was increased only by ~9.5% and most of the threshold increase occurred in the very beginning of the aging. The extrapolated mean-time-to-failure (time to double initial threshold current) is more than a million hours (6,402,903 hours for Device-1 and 26,814,538 hours for Device-2) using the equation in the literature,[21] which is an immense improvement (~270× longer lifetime) over the previous results of 4-6° off-cut Si-based QD lasers.[22, 23] Since slope efficiency (differential quantum efficiency) in the QD lasers also degrades over aging, the bias current to produce an output power of 10 mW at 35 °C was also studied from 10 QD lasers and were plotted in Figure 6 (b). The inset shows the average of the 10 measured devices, and the extrapolated time to double the bias current (100% increase) for 10 mW output power at 35 °C is 3,001,402 hours (~342 years). These lifetime results demonstrate superior reliability of QD lasers with a record-long lifetime for any GaAs-based lasers epitaxially grown on Si.

Conclusion

In summary, we have presented vastly improved 1.3 μm InAs quantum dot lasers epitaxially grown on CMOS-compatible on-axis (001) Si substrates. The high-quality GaAs buffer layer with a threading dislocation density of 8.4 × 10^6 cm^{-2} enabled quantum dot lasers with CW threshold currents as low as 6.2 mA and output powers up to 185 mW. Reducing the threading dislocation density to ~1-2 × 10^6 cm^{-2} in the GaAs buffer layer is expected to improve the quantum dot laser performance further. Optical

characterizations on the low threshold current lasers revealed a low transparency current (~13.1 A/cm^2 per quantum dot layer), low internal loss (2.4 cm^{-1}), and injection efficiency of 87%. Further optical characteristics on modified laser epi structures will be conducted to optimize the number of quantum dot layers and to include p-modulation doping in the active region.

The quantum dot lasers on on-axis (001) Si demonstrated excellent device lifetimes with extrapolated mean-time-to-failure of more than a million hours. We believe that the lowered threading dislocation density in the laser enhanced the device reliability by suppressing recombination-enhanced dislocation climb process.[24] Aging tests with current and temperature acceleration are planned, and light coupling from quantum dot lasers to a waveguide and photodetector via an all-epitaxial approach is a future goal. The significant advancements in the device performance and reliability in this work are very promising for monolithically and 3D integrated photonic circuits on CMOS-compatible on-axis (001) Si substrates.

Supporting Information.

Comparison of quantum dot morphologies grown on GaAs and GaAs/Si, additional light-current-voltage data, comments on quantum dot early gain saturation and mode-sum are available.

Acknowledgements

This research was supported by Advanced Research Projects Agency-Energy (ARPA-E) DE-AR000067 and by Intel Corp. We are also grateful to Kurt Olsson and John English for their assistance in MBE chamber maintenance and Kunal Mukherjee, Alan Liu, Kei May Lau, and Chris Palmstrøm for fruitful discussions.

References

1. Thomson, D.; Zilkie, A.; Bowers, J.; Komljenovic, T.; Reed, G.; Vivien, L.; Marris-Morini, D.; Cassan, E.; Virot, L.; Fedeli, J.; Hartmann, J.; Schmid, J.; Xu, D.; Boeuf, F.; O'Brien, P.; Mashanovich, G.; Nedeljkovic, M., Roadmap on silicon photonics. *Journal of Optics* **2016,** *18* (7).
2. Liu, A.; Zhang, C.; Norman, J.; Snyder, A.; Lubyshev, D.; Fastenau, J.; Liu, A.; Gossard, A.; Bowers, J., High performance continuous wave 1.3 μm quantum dot lasers on silicon. *Applied Physics Letters* **2014,** *104* (4).
3. Chen, S.; Li, W.; Wu, J.; Jiang, Q.; Tang, M.; Shutts, S.; Elliott, S.; Sobiesierski, A.; Seeds, A.; Ross, I.; Smowton, P.; Liu, H., Electrically pumped continuous-wave III-V quantum dot lasers on silicon. *Nature Photonics* **2016,** *10* (5), 307.
4. Wan, Y.; Norman, J.; Li, Q.; Kennedy, M.; Liang, D.; Zhang, C.; Huang, D.; Zhang, Z.; Liu, A.; Torres, A.; Jung, D.; Gossard, A.; Hu, E.; Lau, K.; Bowers, J., 1.3 μm submilliamp threshold quantum dot micro-lasers on Si. *Optica* **2017,** *4* (8), 940-944.
5. Chu, S.; Nakahara, S.; Pearton, S.; Boone, T.; Vernon, S., Antiphase domains in gaas grown by metalorganic chemical vapor-deposition on silicon-on-insulator. *Journal of Applied Physics* **1988,** *64*, 2981-2989
6. Norman, J.; Kennedy, M.; Selvidge, J.; Li, Q.; Wan, Y.; Liu, A.; Callahan, P.; Echlin, M.; Pollock, T.; Lau, K.; Gossard, A.; Bowers, J., Electrically pumped continuous wave quantum dot lasers epitaxially grown on patterned, on-axis (001) Si. *Optics Express* **2017,** *25* (4), 3927-3934.

7. Chen, S.; Liao, M.; Tang, M.; Wu, J.; Martin, M.; Baron, T.; Seeds, A.; Liu, H., Electrically pumped continuous-wave 1.3 μm InAs/GaAs quantum dot lasers monolithically grown on on-axis Si (001) substrates. *Optics Express* **2017,** *25* (5), 4632-4639.
8. Liu, A. Y.; Peters, J.; Huang, X.; Jung, D.; Norman, J.; Lee, M. L.; Gossard, A. C.; Bowers, J. E., Electrically pumped continuous-wave 1.3 μm quantum-dot lasers epitaxially grown on on-axis (001) GaP/Si. *Opt. Lett.* **2017,** *42* (2), 338-341.
9. Jung, D.; Norman, J.; Kennedy, M.; Shang, C.; Shin, B.; Wan, Y.; Gossard, A.; Bowers, J., High efficiency low threshold current 1.3 μm InAs quantum dot lasers on on-axis (001) GaP/Si. *Applied Physics Letters* **2017,** *111* (12).
10. Nemeth, I.; Kunert, B.; Stolz, W.; Volz, K., Heteroepitaxy of GaP on Si: Correlation of morphology, anti-phase-domain structure and MOVPE growth conditions. *Journal of Crystal Growth* **2008,** *310* (7-9), 1595-1601.
11. Shchekin, O.; Deppe, D., 1.3 μm InAs quantum dot laser with T-o=161 K from 0 to 80 degrees C. *Applied Physics Letters* **2002,** *80* (18), 3277-3279.
12. Shtengel, G.; Kazarinov, R.; Belenky, G.; Hybertsen, M.; Ackerman, D., Advances in measurements of physical parameters of semiconductor lasers. *International Journal of High Speed Electronics and Systems* **1998,** *9* (04), 901-940.
13. Cassidy, D. T., Technique for measurement of the gain spectra of semiconductor diode lasers. *Journal of Applied Physics* **1984,** *56* (11), 3096-3099.
14. Andrekson, P.; Olsson, N.; Tanbunek, T.; Logan, R.; Coblentz, D.; Temkin, H., Novel technique for determining internal loss of individual semiconductor-lasers. *Electronics Letters* **1992,** *28*, 171-172.
15. Shtengel, G.; Ackerman, D., Internal optical loss measurements in 1.3-μm InGaAsP lasers. *Electronics Letters* **1995,** *31*, 1157-1159.
16. Casey, H.; Panish, M.; Schlosse, W.; Paoli, T., GaAs-$Al_xGa_{1-x}As$ heterostructure laser with separate optical and carrier confinement. *Journal of Applied Physics* **1974,** *45*, 322-333.
17. Eliseev, P.; Li, H.; Liu, G.; Stintz, A.; Newell, T.; Lester, L.; Malloy, K., Ground-state emission and gain in ultralow-threshold InAs-InGaAs quantum-dot lasers. *IEEE Journal of Selected Topics in Quantum Electronics* **2001,** *7* (2), 135-142.
18. Salhi, A.; Fortunato, L.; Martiradonna, L.; Cingolani, R.; De Vittorio, M.; Passaseo, A., Enhanced modal gain of multilayer InAs/InGaAs/GaAs quantum dot lasers emitting at 1300 nm. *Journal of Applied Physics* **2006,** *100* (12).
19. Salhi, A.; Raino, G.; Fortunato, L.; Tasco, V.; Visimberga, G.; Martiradonna, L.; Todaro, M.; De Giorgi, M.; Cingolani, R.; Trampert, A.; De Vittorio, M.; Passaseo, A., Enhanced performances of quantum dot lasers operating at 1.3 μm. *IEEE Journal of Selected Topics in Quantum Electronics* **2008,** *14* (4), 1188-1196.
20. Salhi, A.; Fortunato, L.; Martiradonna, L.; Todaro, M.; Cingolani, R.; Passaseo, A.; De Vittorio, M., High efficiency and high modal gain InAs/InGaAs/GaAs quantum dot lasers emitting at 1300 nm. *Semiconductor Science and Technology* **2007,** *22* (4), 396-398.
21. Srinivasan, S.; Julian, N.; Peters, J.; Liang, D.; Bowers, J., Reliability of Hybrid Silicon Distributed Feedback Lasers. *IEEE Journal of Selected Topics in Quantum Electronics* **2013,** *19* (4).
22. Liu, A.; Herrick, R.; Ueda, O.; Petroff, P.; Gossard, A.; Bowers, J., Reliability of InAs/GaAs Quantum Dot Lasers Epitaxially Grown on Silicon. *IEEE Journal of Selected Topics in Quantum Electronics* **2015,** *21* (6).
23. Chen, S.; Wu, J.; Tang, M.; Liao, M.; Liu, H., Long lifetime quantum-dot laser monolithically grown on silicon. *2016 IEEE 13th International Conference on Group Iv Photonics (Gfp)* **2016**, 147-148.
24. Kimerling, L., Recombination enhanced defect reactions. *Solid-State Electronics* **1978,** *21*, 1391-1401.

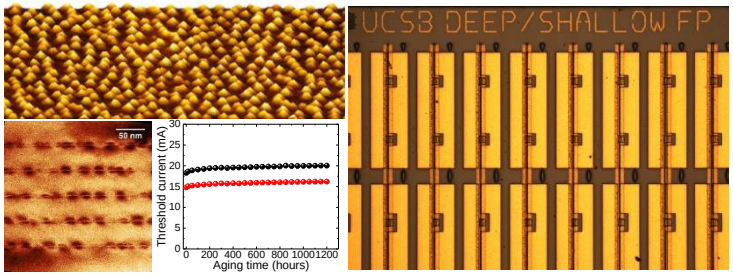
50 nm
Threshold current (mA)
30
25
20
15
10
5
0
0 200 400 600 800 1000 1200
Aging time (hours)
UCSB DEEP/SHALLOW FP

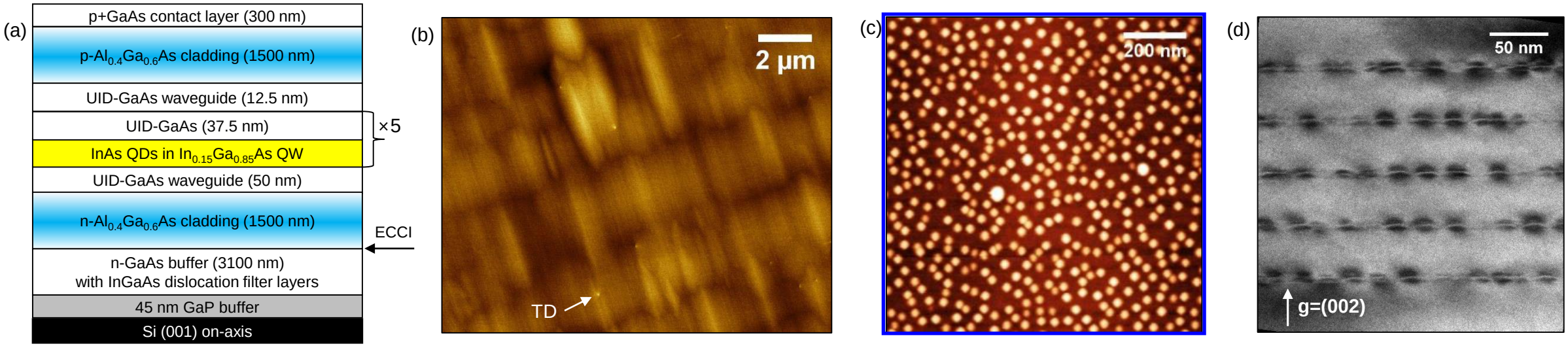
(a)
p+GaAs contact layer (300 nm)
p-Al0.4Ga0.6As cladding (1500 nm)
UID-GaAs waveguide (12.5 nm)
UID-GaAs (37.5 nm)
InAs QDs in In0.15Ga0.85As QW
×5
UID-GaAs waveguide (50 nm)
n-Al0.4Ga0.6As cladding (1500 nm)
ECCI
n-GaAs buffer (3100 nm)
with InGaAs dislocation filter layers
45 nm GaP buffer
Si (001) on-axis
(b)
2 µm
TD
(c)
200 nm
(d)
50 nm
g=(002)

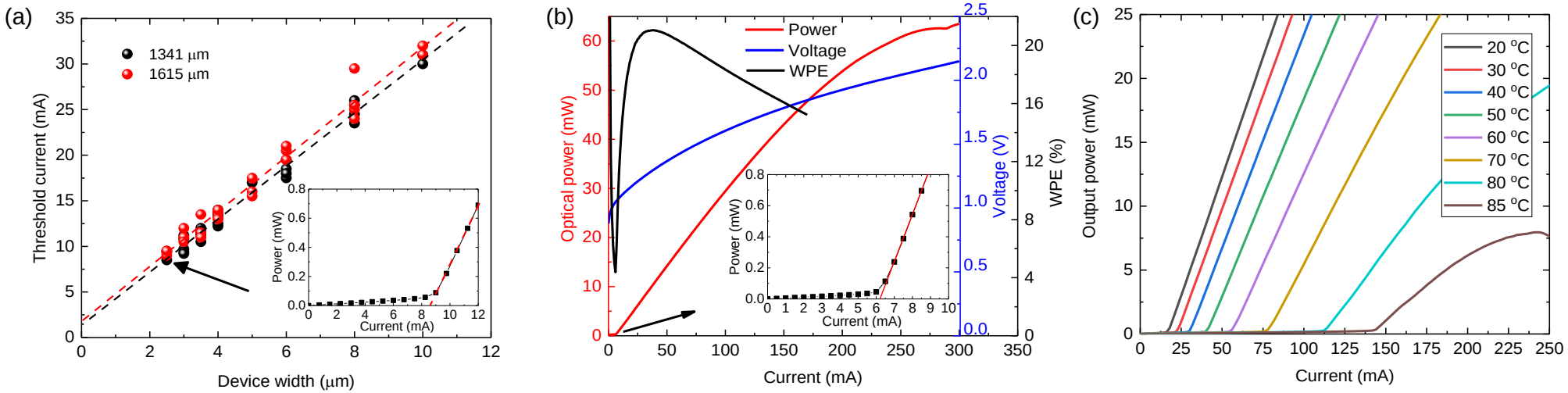
(a)
1341 μm
1615 μm
Threshold current (mA)
Device width (μm)
Power (mW)
Current (mA)
(b)
Power
Voltage
WPE
Optical power (mW)
Voltage (V)
WPE (%)
Current (mA)
Power (mW)
Current (mA)
(c)
20 °C
30 °C
40 °C
50 °C
60 °C
70 °C
80 °C
85 °C
Output power (mW)
Current (mA)

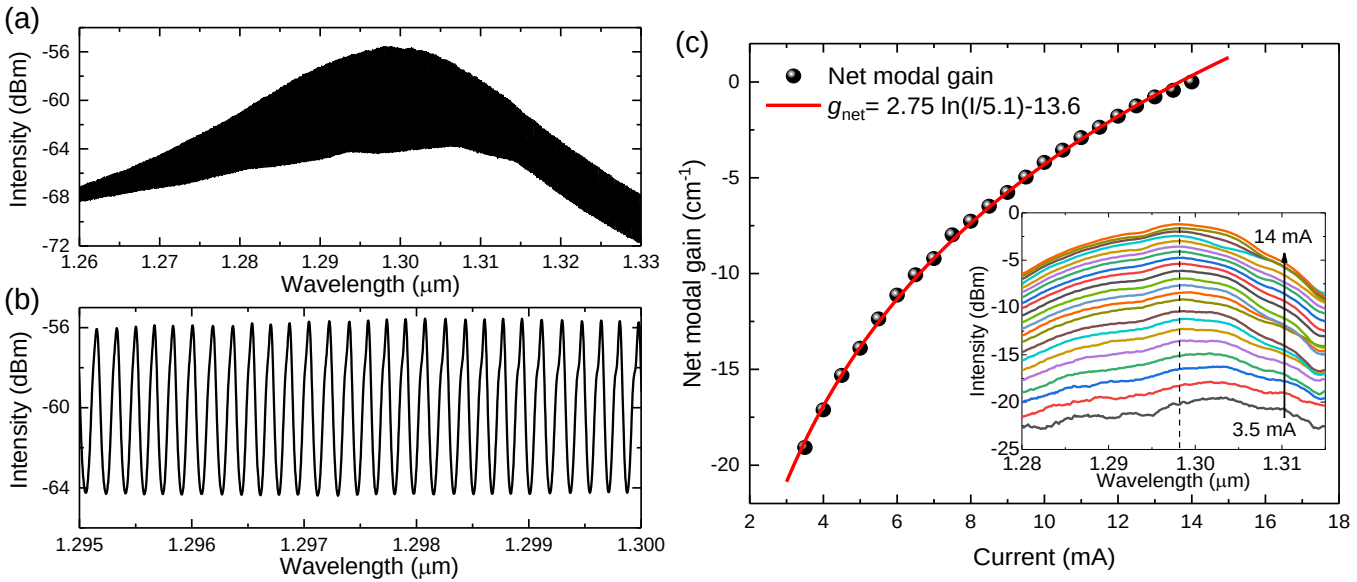
(a)
Intensity (dBm)
-56
-60
-64
-68
-72
1.26
1.27
1.28
1.29
1.30
1.31
1.32
1.33
Wavelength (μm)
(b)
Intensity (dBm)
-56
-60
-64
1.295
1.296
1.297
1.298
1.299
1.300
Wavelength (μm)
(c)
Net modal gain
g_{net}= 2.75 ln(I/5.1)-13.6
Net modal gain (cm^{-1})
0
-5
-10
-15
-20
2
4
6
8
10
12
14
16
18
Current (mA)
Intensity (dBm)
14 mA
3.5 mA
1.28
1.29
1.30
1.31
Wavelength (μm)

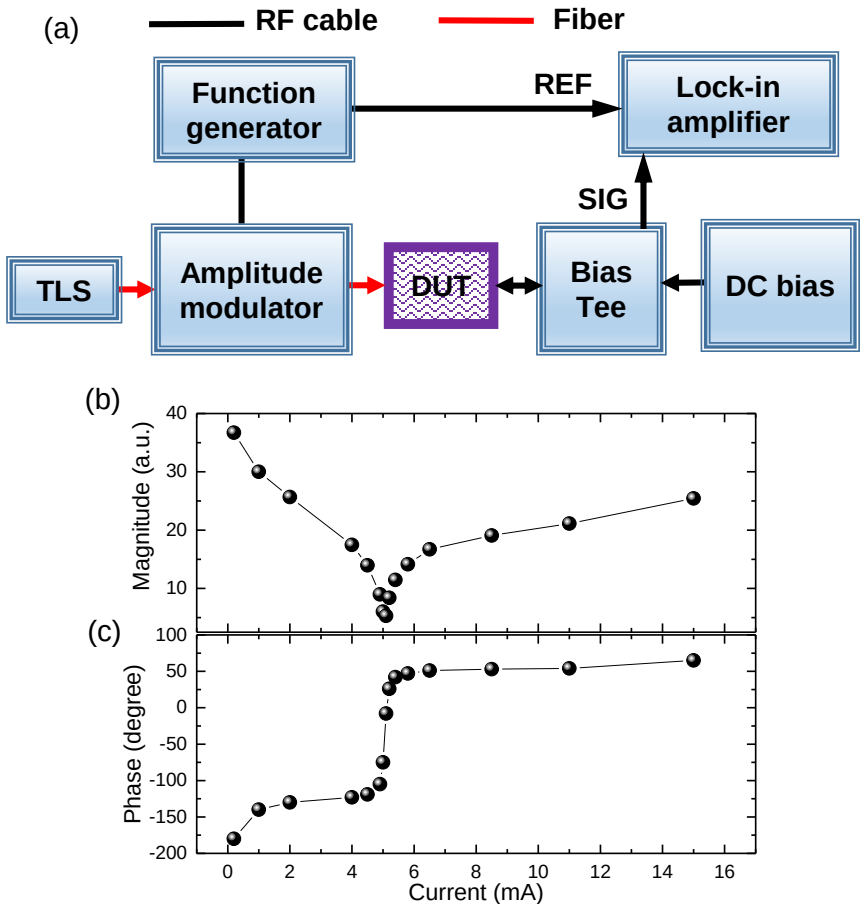
(a)
RF cable
Fiber
Function generator
REF
Lock-in amplifier
SIG
TLS
Amplitude modulator
DUT
Bias Tee
DC bias
(b)
Magnitude (a.u.)
40
30
20
10
(c)
Phase (degree)
100
50
0
-50
-100
-150
-200
0
2
4
6
8
10
12
14
16
Current (mA)

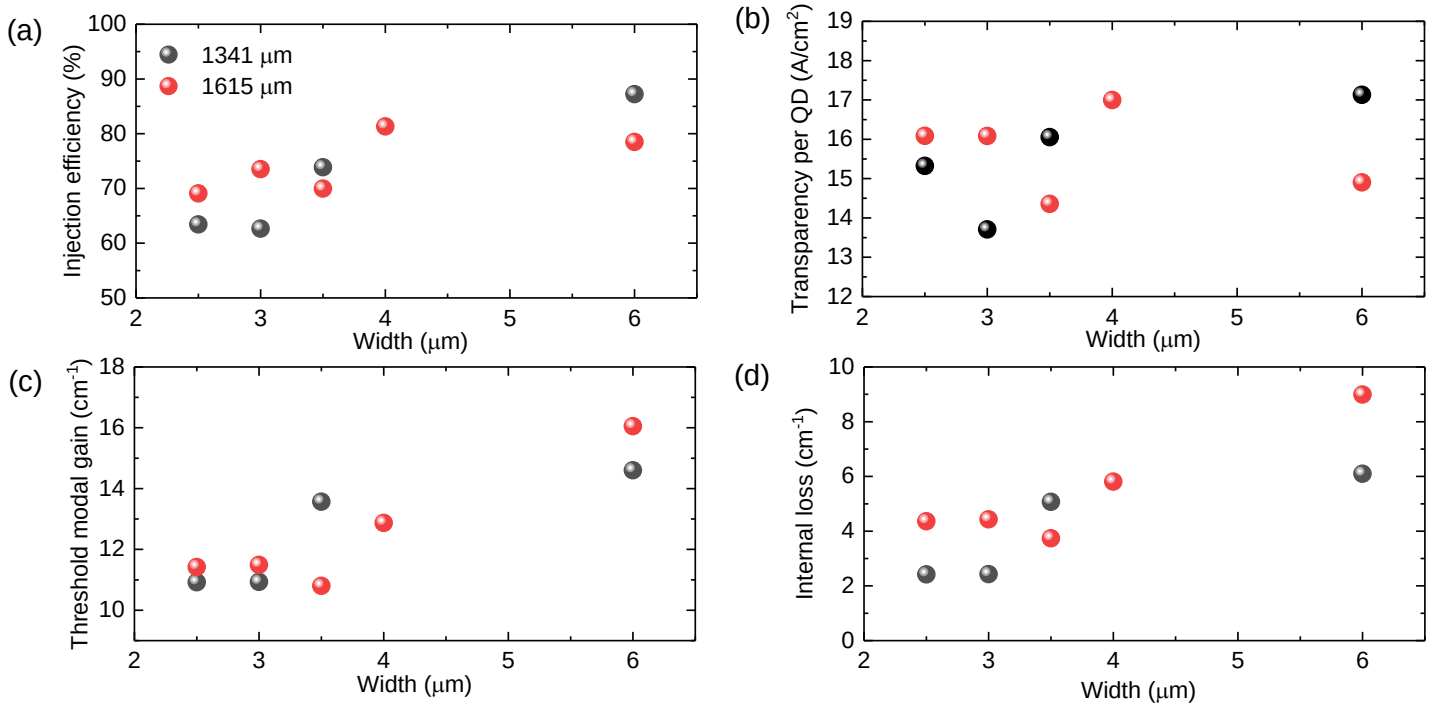
(a)
Injection efficiency (%)
1341 μm
1615 μm
Width (μm)
(b)
Transparency per QD (A/cm²)
Width (μm)
(c)
Threshold modal gain (cm⁻¹)
Width (μm)
(d)
Internal loss (cm⁻¹)
Width (μm)

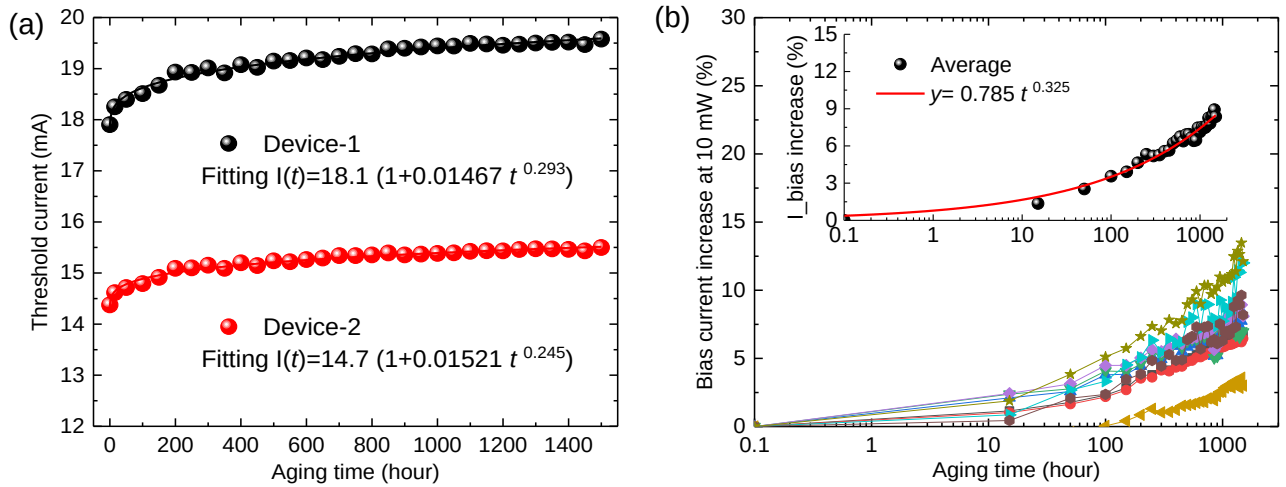
(a)
Threshold current (mA)
Aging time (hour)
Device-1
Fitting I(t)=18.1 (1+0.01467 t 0.293)
Device-2
Fitting I(t)=14.7 (1+0.01521 t 0.245)
(b)
Bias current increase at 10 mW (%)
Aging time (hour)
I_bias increase (%)
Average
y= 0.785 t 0.325